September 1992 Report No. STAN-CS-92-1441

Motion Planning in Stereotaxic Radiosurgery

by

A. Schweikard, J. Adler, J. Latombe

Department of Computer Science

Stanford University

Stanford, California 94305

Motion Planning in Stereotaxic Radiosurgery

Achim Schweikard John R. Adler* Jean-Claude Latombe
Robotics Laboratory, Department of Computer Science
Stanford University, Stanford, CA 94305, USA

Abstract

Stereotaxic radiosurgery is a procedure which uses a beam of radiation as an ablative surgical instrument to destroy brain tumors. The beam is produced by a linear accelerator which is moved by a jointed mechanism. Radiation is concentrated by crossfiring at the tumor from multiple directions and the amount of energy deposited in normal brain tissues is reduced. Because access to the tumor is obstructed along some directions by critical regions (e.g., brainstem, optic nerves) and most tumors are not shaped like spheres, planning the path of the beam is often difficult and time-consuming. This paper describes a computer-based planner developed to assist the surgeon generate a satisfactory path, given the spatial distribution of the brain tissues obtained with medical imaging. Experimental results with the implemented planner are presented, including a comparison with manually generated paths. According to these results, automatic planning significantly improves energy deposition. It can also shorten the overall treatment, hence reducing the patient's pain and allowing the radiosurgery equipment to be used for more patients. Stereot axic radiosurgery is an example of so-called "bloodless surgery". Computer-based planning techniques are expected to facilitate further development of this safer, less painful, and more cost effective type of surgery.

Key words: Stereotaxic radiosurgery, geometric reasoning, path planning.

Acknowledgments: The authors thank Rick Cox, Bill Haneman, Paul Hemler, Todd Koumrian, and David Martin from the Stanford Medical Center for making their radiosurgical dosimetry vprogram available to them and discussing various aspects of treatment planning.

*Department of Neurosurgery, School of Medicine.

1. INTRODUCTION

The term stereotaxic radiosurgery refers to a procedure which uses an intense focused beam of radiation as an ablative surgical instrument. The treatment makes use of the spatial information provided by Computed Tomography (CT) and Magnetic Resonance Imaging (MRI). Several leading medical schools worldwide have recently reported dramatic success with such techniques mainly in the outpatient treatment of both operable and inoperable brain tumors. In addition to being safer than conventional operations, this procedure is much less expensive.

In brain surgery, there are three types of radiosurgical techniques which are distinguished by radiation source:

- Radiation by a static beam of heavy particles (protons or helium ions) generated by a synchrocyclotron.
- Radiation by an array of static Co^{60} sources (Gamma-knife).
- Radiation by a photon beam produced by a linear accelerator moved by a jointed mechanism.

Due to its greater flexibility and relatively low cost, the third technique is most frequently used. A standard system using this technique is the modified Brown-Roberts-Wells-System (LINAC System) [8, 11]. This system consists of a jointed mechanism with 5 degrees of freedom which moves a 6 MeV photon source generating a cylindrical beam of adjustable radius. During treatment, the accelerator moves around the patient's head along a predefined path, so that the radiation is concentrated by crossfiring at the tumor from multiple directions and the amount of energy deposited in normal tissues is relatively small. However, the beam access to the tumor is often obstructed along some directions by particularly critical and/or sensitive brain structures, e.g., brainstem, carotid artery, optic nerves and optic chiasm, whose over-radiation may result in severe side effects such as paralysis or blindness. As a consequence, the path of the beam should be generated so as to minimally irradiate these regions. The fact that most tumors are not shaped like spheres complicates further the problem of finding an appropriate motion for the beam. Currently, path planning is done manually, although the complexity of the geometric reasoning involved suggests that it might be done better and quicker by a computer.

The overall treatment consists of the following steps:

1. A metal frame, called stereotaxic frame, is attached to the patient's skull using screws placed under local anaesthesia. The position of the frame relative to the jointed mechanism is fixed and known with high precision.

2. CT and MR images are obtained and analyzed with the frame attached. The locations of both the tumor and the critical regions are determined with respect to the frame.

3. A path of the radiation beam is planned based on this spatial information. The dose distribution corresponding to this path is computed by a dosimetry program. If the surgeon finds the distribution acceptable, the treatment proceeds to step 4, otherwise another path is generated.

4. The jointed mechanism moves the beam along the path accepted by the surgeon.

This procedure is quite long; it takes of the order of 30 minutes, l-2 hours, 2-3 hours, and l-2 hours for steps 1, 2, 3, and 4, respectively. The patient is conscious throughout all steps, and the stereotaxic frame, which remains attached to his/her head (since the correspondence between the images and the jointed mechanism must be maintained), is very painful. Shortening the procedure is thus important to reduce the patient's pain. It would also allow the treatment of more patients with the same equipment. In this context, various computer techniques can be applied. In particular, in step 2, image interpretation software can be used to automatically locate the tumor and the critical regions. In step 3, motion planning techniques can be used to generate appropriate beam paths.

Image interpretation techniques to locate regions of interest in the brain have been reported in the literature (e.g., see [1, 6]). In this paper we investigate motion planning methods for generating beam paths. We describe an implemented planner developed to assist surgeons generate satisfactory paths. We present preliminary experimental results obtained with this planner. These results show that motion planning software can both significantly reduce energy deposition in critical tissues and dramatically shorten the duration of step 3.

Other image-guided systems which do not use radiosurgery have been introduced in [5, 9]. The system in [5] is used for inserting electrodes or radioactive seeds into a patient's brain with high accuracy; the electrode or seed is moved to an appropriate entry position by a six degree-of-freedom robot and then moved into its final placement in the brain by the surgeon. A robotic system designed to create femoral cavities that are precisely shaped and positioned for inserting uncemented prostheses is described in [9]. Motion planning techniques could also be beneficial to the development of these systems. However, the planning issues they raise are different from those of radiosurgery.

The path planning problem considered in this paper also departs significantly from more classical robot motion planning [4], where the goal is to move an object (the robot) to a goal configuration among obstacles.

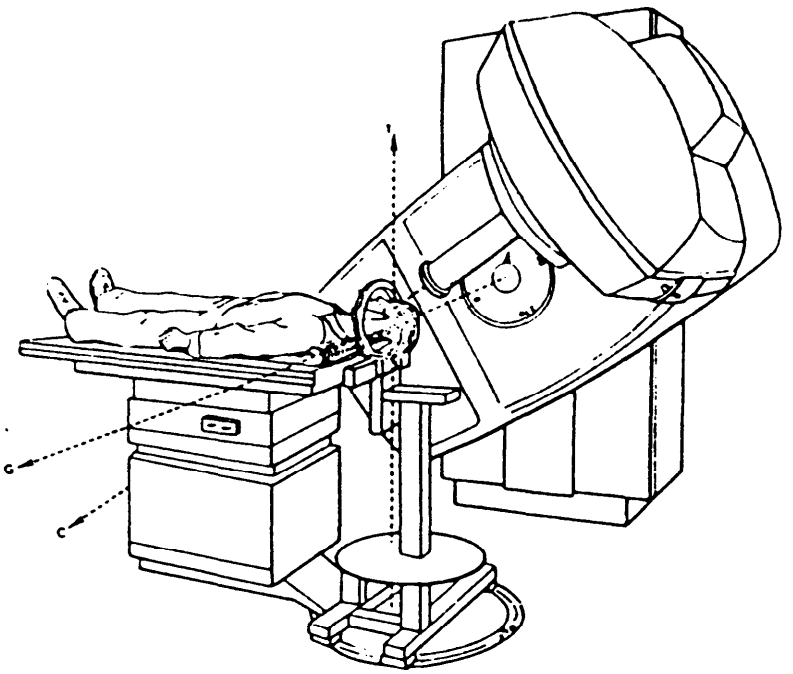

Figure 1: Schematic of LINAC system [11]

Section 2 presents the kinematics of the LINAC system and the standard treatment with this equipment. Sections 3 through 5 describe the geometric methods used in our planner. Sections 6 and 7 discuss the implementation of the planner and experimental results.

2. LINAC System

The radiosurgery equipment used in our work is the LINAC system (8, **11)** shown in Fig. 1. It consists of a floor stand (couch) with four joints and a gantry with a revolute joint. The position of the floor stand can be adjusted with three prismatic joints. Its orientation in the horizontal plane is set by a revolute joint about the axis designated by T in Fig. 1. The linear accelerator can be moved by rotating the gantry about the axis denoted by G. The beam central axis is denoted by C. The three axes T, G, and C always intersect in one point. While the accelerator is rotated, the floor stand joints remain fixed, so that the beam can only span vertical angular sectors. The radius of the beam generated by the accelerator can be adjusted by inserting a lead collimator into the accelerator. The beam can be turned on and off during the

motion.

The standard treatment using this equipment is the following. Assume first that the tumor is a ball $\mathcal{T}$. The prismatic joints in the floor stand are adjusted such that the intersection point of **T, G** and C coincides with the center of 7. The beam radius is set to the radius of $\mathcal{T}$. The revolute joint of the floor stand (axis T) is set to a fixed angular position α_1. In this position the gantry is moved around G between two orientations β_1 and β_1', while the beam is activated. In this way, the beam spans a vertical angular sector whose apex is the center of $\mathcal{T}$. Furthermore, throughout the motion, 7 is inside the beam. The floor stand revolute joint is then set to a new angular position α_2 and a second arc (β_2, β_2') is generated by moving the gantry, and so on. The standard motion procedure described in [8] consists of four such arcs. The angle between any two planes containing these arcs should be large enough so that the volumes swept by the beam when it moves along the various arcs have small intersection outside the tumor. It is thus ensured that the dose inside 7 largely exceeds the dose absorbed by surrounding tissues. Energy deposition can be computed by a standard dosimetry program which is currently in clinical use. If this computation shows too large a dose to critical regions, the 4-arc path is modified by changing the floor stand angles, the gantry motion ranges, and/or the beam intensity along each arc.

When the tumor is not sphere-shaped, it is approximated as a collection of non-intersecting spheres. Each sphere is treated independently as described above.

The planner described below directly applies to this LINAC system and generates standard 4-arc paths. However, it is more general. In particular, with the same system kinematics, it can generate paths with an arbitrary number of arcs, which potentially allows a better distribution of energy in the brain, especially when the tumor and critical regions are adjacent to one another. Simple extensions (not described in this paper) would also allow the planner to deal with a less constrained mechanical system.

The constrained kinematics of the LINAC system and the additional restrictions brought by the standard 4-arc treatment have two main motivations: (1) protect the patient against collision with the moving gantry, and (2) facilitate manual path planning, without significantly impairing the overall quality of the treatment. However, better energy deposition could be achieved by using a more versatile kinematic system. Then the combined use of classical robot path planning techniques to prevent collisions and sensory equipment to anticipate them could ensure satisfactory protection of the patient. Automatic path planning techniques such as the ones described in this paper could address the increased difficulty of treatment planning.

3. GEOMETRY OF THE BEAM CONFIGURATION SPACE

3.1. BEAM CONFIGURATION SPACE

Let us assume that the tumor is modeled as a spherical ball 7 of radius ***r*** centered at the coordinate origin ***0.*** A ***configuration*** of the radiation beam is defined as the orientation of its central axis C when this axis goes through 0. In the following, we assume that the energy distribution along the beam is constant; hence, any two opposite orientations of the beam are equivalent. We can then represent a beam configuration by the two antipodal points where its central axis intersects the unit sphere S^2 centered at 0. The set of all beam configurations, i.e., the beam's ***configuration space,*** is thus represented as the sphere S^2 with antipodal points identified.

The kinematics of the LINAC system constrains the beam configuration to move along arcs of great circles of S^2 contained in vertical planes. A path of the accelerator is thus defined as a series of such arcs.

Our planning techniques treat critical regions as obstacles that should not be intersected by the beam. This leads to precomputing the map of each critical region into S^2 as a set of forbiden configurations called ***C-obstacle.*** The complement of the C-obstacles in S^2 is called the ***free space.***

3.2. C-OBSTACLES

Let C_i, i $= 1, \ldots, m,$ denote the critical regions of the brain. Each region C_i maps into S^2 as follows:

We grow C_i isotropically by the radius ***r*** of 7 (i.e., the radius of the beam); this yields a grown region C_i'. Intuitively, C_i' is obtained by moving a ball of diameter ***r*** to all placements where it is in contact with C_i, without overlapping it; C_i' is equal to C_i enlarged by the volume swept out by the ball. More formally, we have:

$$C_i' = C_i \oplus B_r = \{c + b \mid c \in C_i, b \in B_r\},$$

where B_r is the ball of radius ***r*** centered at the coordinate origin 0 and $\oplus$ denotes the Minkowski set sum.

Hence, if the beam central axis does not cross the enlarged region C_i', then the beam does not intersect C_i. The central projection of C_i' from 0 into S^2 gives the C-obstacle corresponding to C_i. Note that each C-obstacle consists of two antipodal regions.

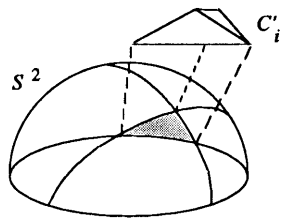

Figure *2:* Construction of free space

3.3. Computation of Free Space

The following simple technique can be used to compute an approximation of free space: Let C_i, i = 1,. . . , ***m,*** be polyhedra approximating the critical regions, and D_r be a cube of edge length $2r$, centered at 0, bounding the spherical tumor 7. We construct each C'_i as $C_i \oplus D_r$, rather than $C_i \oplus B_r$. C'_i is then a polyhedron whose computation is studied in [7, 3]. This approximation yields a particularly simple projection of C'_i into S^2. Indeed, each edge ***E*** of C'_i maps to an arc of great circle which is the intersection of the plane containing 0 and ***E*** with S^2. The set of edges of all grown regions C'_i thus determines a collection of great circles which partition S^2 into an arrangement of regions (Fig. 2). The free space is the union of a subset of these regions.

Let n be the total number of vertices of the polyhedra $C_1, \ldots, C_m$. The grown regions C'_i can be computed in O(n) time using the algorithm described in [3]. They have a total of $0(n)$ vertices and thus yield ***O(n)*** great circles in S^2 forming an arrangement of $O(n^2)$ regions. This arrangement can be computed in $O(n^2)$ time [2].

Example: The computation of free space is illustrated in Fig. 3 with a simple two-dimensional example. (The beam configuration space is then the unit circle S^1.) In (a), C_1 and C_2 are polygons approximating critical regions, C is the beam central axis at some arbitrary free configuration of the beam, and D_r is the bounding square containing the tumor disc 7. In (b), C'_1 and C'_2 are the grown regions corresponding to C_1 and C_2. Each grown region is projected into S^1 as two antipodal arcs (the C-obstacles). The complement of these arcs, i.e., the two antipodal arcs shown in bold lines, represents free space.

In the following, we assume that C-obstacles and free space have been computed using the above approximation. They are therefore bounded by arcs of great circles.

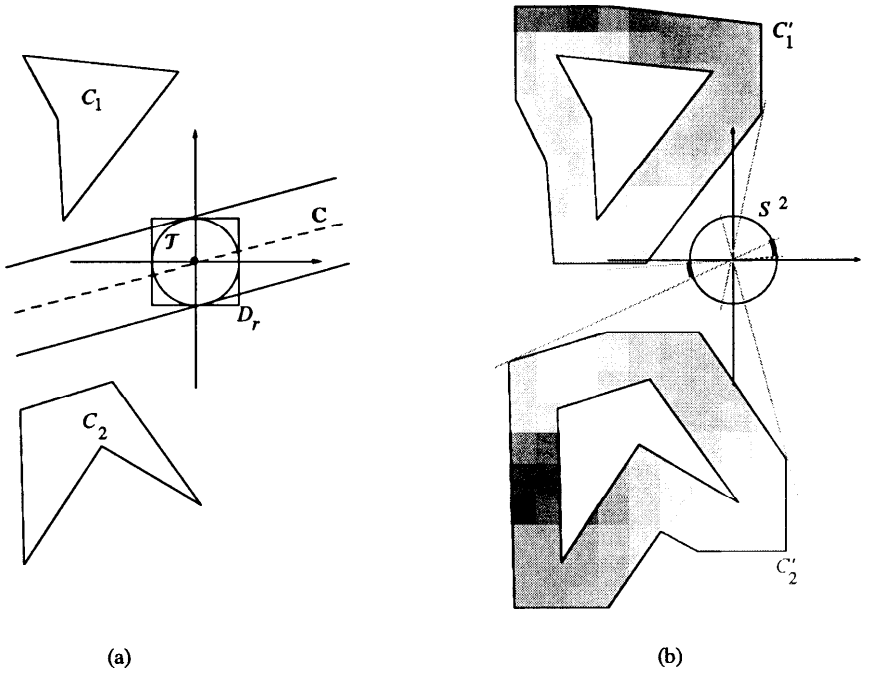

Figure 3: Computation of free configurations in a two-dimensional example

4. COMPUTATION OF VERTICAL FREE ARCS

4.1. CHARACTERIZATION OF GREAT CIRCLES

Let g be any great circle of S^2. We can represent g by two antipodal points of a sphere DS^2, the ***dual sphere*** of S^2, defined as the extremities of the two opposite unit vectors erected at 0 and normal to the plane containing g.

Let e be an edge (arc of great circle) of a C-obstacle, and u and v be its endpoints. Let G(u) be the set of all great circles of S^2 containing u. This set maps into DS^2 as a great circle ***n(u).*** In the same way the great circles of S^2 containing v map to a great circle ***n(v)*** of DS^2. The two circles ***n(u)*** and ***n(v)*** partition DS^2 into four regions. Two of these regions represent the set of great circles in S^2 that intersect the arc e.

Consider the C-obstacle edges in S^2. The set of great circles corresponding to the endpoints of these edges partition DS^2 into an arrangement ***A*** of regions. Let ***R*** be any such region and ***p*** be any point in ***R.*** The great circle of S^2 corresponding to ***p*** intersects a possibly empty set ***a(R)*** of C-obstacle edges. The region ***R*** is ***regular*** in the following sense: The set a(R) is independent of the choice of ***p*** in ***R.*** We call it

the ***characteristic set*** of ***R.***

The arrangement ***A*** is created by ***O(n)*** great circles. It contains $O(n^2)$ regions and can be computed in $O(n^2)$ time (as above, ***n*** is the total number of vertices of the critical regions). The characteristic set of any region in ***A*** can be computed in ***O(n)*** time. By noticing that the characteristic set undergoes minor changes between two adjacent regular regions, which can be computed in constant time, it is possible to generate all characteristic sets in $O(n^2)$ time.

However, the LINAC system can only move the beam source along arcs of vertical great circles. Although the computation of ***A*** and the characteristic sets can be useful for a more versatile mechanical system, it is too general here.

4.2. Free Vertical Great Circles

Vertical great circles of S^2 are represented by points of the horizontal circle H of DS^2. The intersection points of H with the circles of the arrangement ***A*** decompose H into arcs. Let $L = (s_1, s_2, \ldots)$ be the sorted list of these arcs. All vertical great circles represented by points in the same arc s_i intersect the same C-obstacle edges (possibly none). Let $r(s_i)$ denote the number of C-obstacle edges intersected by the great circle of S^2 represented by any point of s_i; $r(s_i)$ is equal to the size of the characteristic set of the region of ***A*** containing s_i (although it can be computed more directly). If $r(s_i) = 0$ then all points in s_i represent free great circles of S^2. By scanning the list L of arcs of H, we can identify all arcs s where ***r(s)*** reaches 0 and report the sublist of these arcs, which represents all free vertical great circles of S^2.

As mentioned above, this computation does not require the precomputation of the characteristic sets of the regions of ***A.*** The intersections of H with the circles generating ***A*** can be computed in ***O(n)*** time. The sorted list L is thus produced in O(nlog ***n)*** time. The number $r(s_1)$ can be computed directly in ***O(n)*** time. The arcs s_1 and s_2 are separated by a point where H intersects a great circle of ***A.*** By analyzing this intersection, one can compute $r(s_2)$ from $r(s_1)$ in constant time. In the same way, each new number $r(s_i)$ can be computed in constant time from $r(s_{i-1})$. Hence, the list of arcs s verifying ***r(s)*** = 0 is generated in ***O(n*** log ***n)*** time.

4.3. Free Vertical Arcs of Given Length

In many cases, however, there exist no free vertical great circles or the existing ones do not have sufficient angular distance between them. Therefore, it may be more interesting to compute vertical great circles in which free arcs have a cumulated length greater than some specified value K. When the accelerator is moved along

such a circle, the beam must alternatively be turned on and off.

The vertices of the free space in S^2 map to a collection of great circles of DS^2. These circles partition H into a list $L' = (s'_1, s'_2, \ldots)$ of arcs ($L \subseteq L'$). Consider any arc s'_i in this list. All vertical great circles of S^2 represented by the points of s'_i intersect the same C-obstacle edges ***in the same order.*** We decompose every arc s'_i into subarcs such that when a point p varies from one extremity of any subarc to the other, the total length of free arcs in the great circle of S^2 represented by p increases or decreases monotonically. Each subarc of H thus contains at most one connected segment representing great circles containing free arcs with total length greater than the given threshold K.

The number of segments thus extracted from H is polynomial in n. The computation also requires polynomial time. It involves finding the zeros of polynomial equations. We will not discuss this issue here. The implemented planner makes use of an approximate technique based on discretizing H (see Section 5).

One may alternatively consider great circles containing a connected free arc whose length is greater than some value. The computation of such great circles can be done with a technique similar to the above.

5. PATH PLANNING

A path of the LINAC system consists of a series of arcs (connected or not) contained in different vertical great circles. We consider the path planning problem defined by three parameters: the number k of great circles, the minimal cumulative length K of the free arcs in each great circle, and the minimal angle w between the planes of any two great circles. The planner generates a path as follows:

We give an arbitrary orientation to the horizontal great circle H of DS^2. Let $(s^\kappa_1, s^\kappa_2, \ldots)$ be the sorted list of the arcs of H representing the vertical great circles of S^2 whose free arcs have a total length greater than K. We must find a series of k points $p_1, \ldots, p_k$ in these arcs such that the angle $\omega(p_i, p_j)$ between the vertical planes containing the great circles represented by any two points p_i and p_j is smaller than w. (Note that $\omega(p_i, p_j)$ is equal to the angular distance between p_i and p_j in H.)

Assume that the points p_i have been computed. If none coincides with an endpoint of an arc s^κ_j, then we can move all the points p_i simultaneously, in the direction opposite to that of H, until one reaches an endpoint of an arc s^κ_j. Therefore, to compute the points p_i, we can assume that one point coincides with the first endpoint of an arc s^κ_j (the arc being oriented as H).

We begin by placing the point p_1 at the first endpoint of an arbitrarily selected

arc $s_{j_1}^{\kappa}$. We then move in the direction of $\boldsymbol{D}$ and place p_2 within an arc $s_{j_2}^{\kappa}$ (possibly, equal to $s_{j_1}^{\kappa}$), such that the angular distance between p_1 and p_2 is minimal, but larger than w. After placing p_1 and p_2, the remaining points are positioned in the same way. Whenever a new point is positioned, it is also verified that its angular distance to p_1 is greater than or equal to w. If no appropriate placement is found for any point p_2 through p_k, p_1 is selected at the first endpoint of another arc and the construction is repeated.

If the planner terminates successfully, it provides a set of $\boldsymbol{k}$ great circles satisfying the input constraints, along with the free arcs in each great circle. If it fails to find a path, one can modify the constraints, i.e., the values of $\boldsymbol{k}$, K, and w.

Assume that the arcs s_j^{κ} in $\boldsymbol{H}$ have already been computed. Let $\boldsymbol{q}$ be the number of these arcs. For a given position of p_1, the placement of every point p_i takes 0(log $\boldsymbol{q}$) time. The placement of all points, if possible, thus takes $\boldsymbol{O(k}$ log $\boldsymbol{q)}$ time. In case of successive failures, the process is repeated up to $\boldsymbol{q}$ times, yielding a total planning time of $\boldsymbol{O(kq}$ log $\boldsymbol{q)}$. If $K = 2\pi$ (i.e., if we are only interested in great circles), then $\boldsymbol{q} \in \boldsymbol{O(n)}$. If $K < 2\pi$, then $\boldsymbol{q}$ has a higher-degree polynomial dependence on $\boldsymbol{n}$.

Alternatively, a problem can be defined so that each great circle contains a connected free arc of length greater than or equal to K. The selection of the points p_i is done in the same way as above.

6. IMPLEMENTATION

An interactive planner based on the techniques described above has been implemented to compute appropriate multi-arc paths for a LINAC-based radiosurgical system. The software is written in C and runs on a Silicon Graphics workstation. The planner has been connected with dosimetry and imaging software already in use with the stereotaxic system at Stanford Medical Center.

CT and MR images give the anatomy of the brain in parallel axial cross-sections separated by 3 to 5 mm. The critical regions in each cross-section are delineated by polygons. These polygons are then "thickened" by the distance between cross-sections, thus yielding a polyhedral approximation of every critical region. Currently, the delineation operation in each cross-section is done manually.

The planner operates as described above with the difference that the horizontal great circle $\boldsymbol{H}$ in DS^2 is discretized into 128 equidistant points. For every point $\boldsymbol{p}$ in the discretization of $\boldsymbol{H}$, the planner computes the set of free arcs in the great circle of S^2 represented by $\boldsymbol{p}$ and the total length (or maximal length) of these arcs. This leads the planner to compute each arc s_j^{κ} as a list of points, instead of a continuous

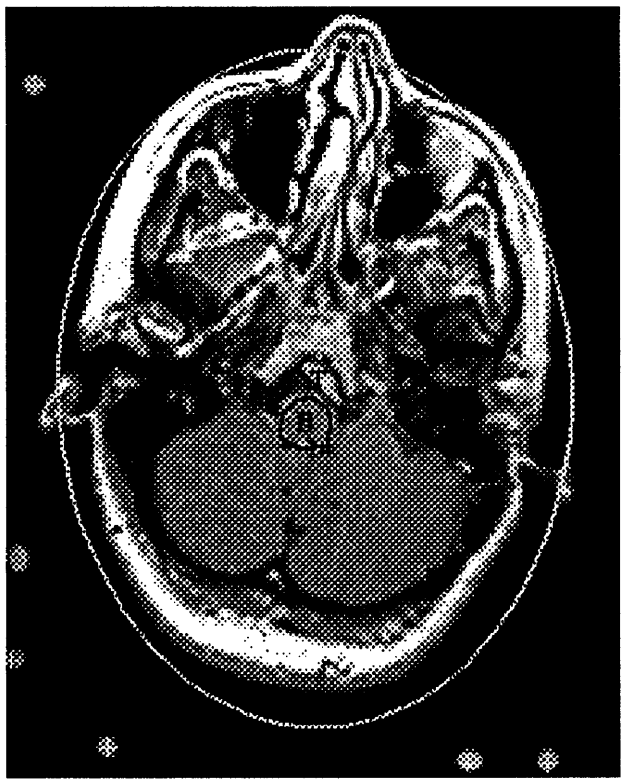

Figure 4: Axial cross-section of the brain in Case **1**

segment. The rest of the planner operates in the same way as above.

When the tumor cannot be well represented by a single sphere, it is approximated by several non-intersecting spheres. A distinct path is generated for each such sphere. To simplify the use of the planner and potentially improve the subsequent treatment, a geometric method for approximating tumors by a given number of spheres was implemented. This method is based on an algorithm described in [10] for finding the smallest sphere containing a set of points in space.

The current planner either returns a path or indicates failure. If it returns a path, the dosimetry program is run and computes the energy deposition in the brain tissues that will result from the execution of this path. If the surgeon does not find this distribution acceptable, the planner is called back with different parameters (k, K, and w). If the planner fails to return a path, it can also be called back with different parameters.

The planner incorporates several straightforward improvements. For example, when it finds a path, it can iteratively rotate the ***k*** vertical planes containing the

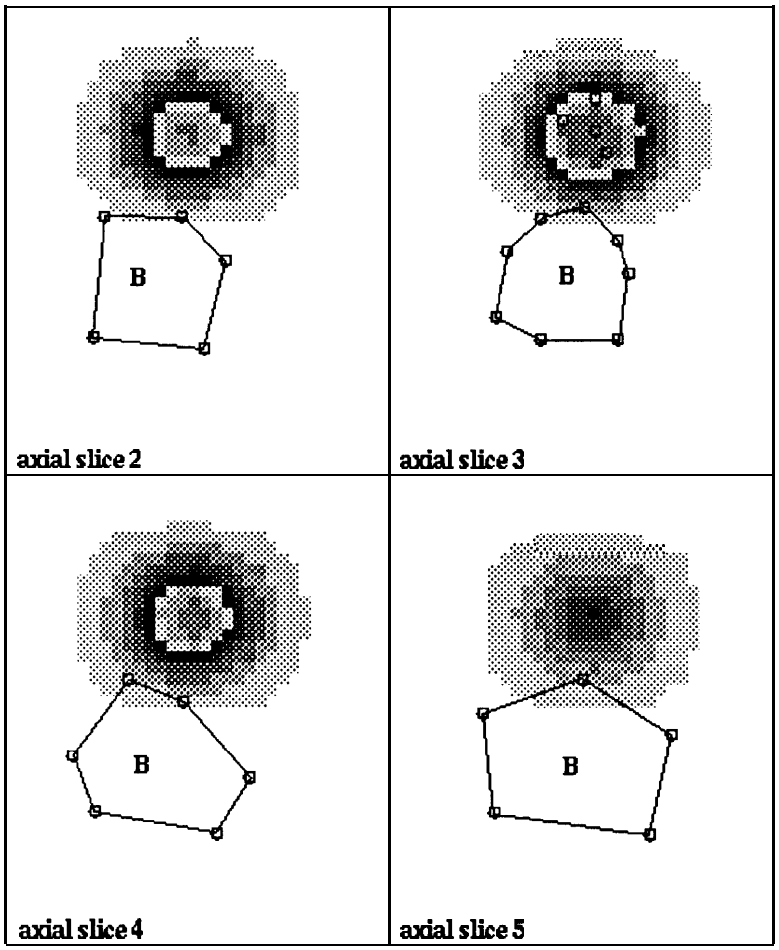

Figure 5: Dose distribution for the manually generated path in Case **1**

planned arcs to maximize the minimal length of free arcs in each one. When it fails to find a path satisfying the constraints, it can find, by bisection, the maximal w for which there is a path.

Currently, we assume that the beam intensity is the same for the ***k*** arcs and tuned proportional to the inverse of the total length of these arcs. A potential improvement of the planner, which we have not explored yet, is to allow for a different beam intensity along each arc.

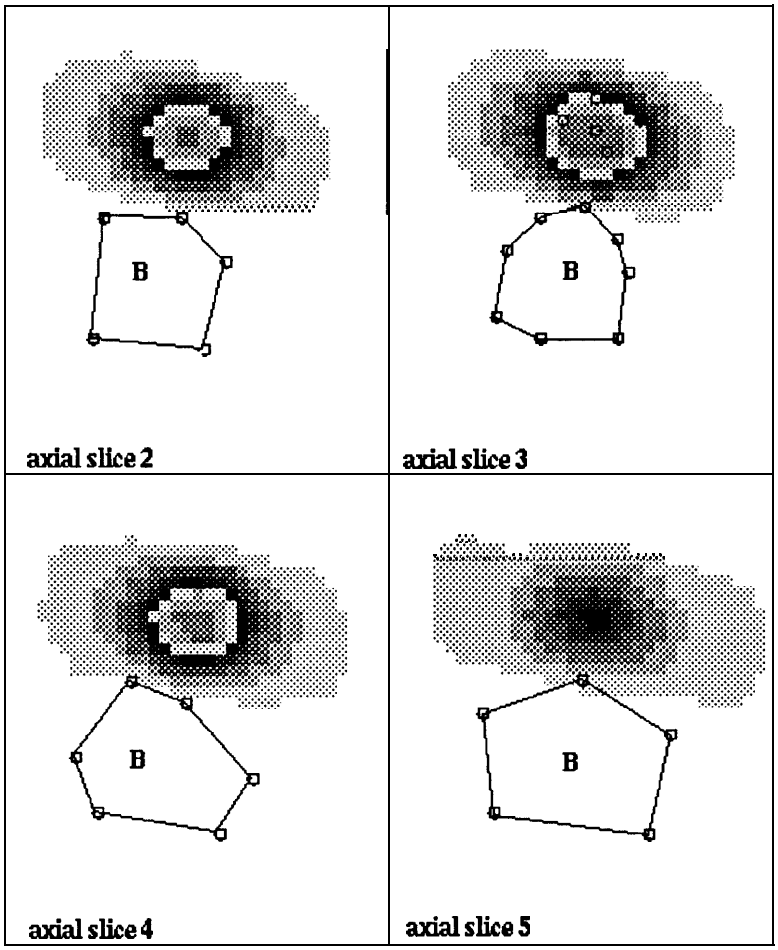

Figure 6: Dose distribution for the automatically planned path in Case **1**

7. EXPERIMENTS

In order to carry out a preliminary evaluation of the planner, we ran it on 11 cases which had previously been treated with the stereotaxic system at the Stanford Medical Center. In each case, the dose distribution for the path computed by the planner was compared to the distribution for the original path which had been generated manually. We report two representative cases below.

To make comparison with manual planning realistic, the planner was run with k = 4 and an initial value of w equal to the standard 45 degrees. We also requested the planner to find great circles containing a connected free arc of length greater than some K. When the planner found a path, this path was automatically optimized as

explained above. When the planner failed, w was determined by bisection. In all cases, the planner took on the order of l-2 minutes to generate a path.

The planner was also used to generate paths with more than 4 vertical arcs. Interestingly, this usually led to relatively small improvements. On the other hand, limited additional experiments have shown that in some cases the restriction to vertical arcs impairs the dose distribution (see Conclusion).

7.1. CASE 1

Fig. 4 shows the CT image of an axial cross-section of the brain. A single critical region (brain stem) is delineated by a polygon B. The tumor is designated by ***T.*** Both the manually generated path and the computed path consist of 4 connected arcs in different planes. They were generated for a tumor approximated by one sphere of radius 10 mm.

Fig. 5 shows the energy deposition computed by the dosimetry program in four cross-sections distant by 3 mm for the manually generated path. Fig. 6 shows the deposition computed for the path generated by the planner. In both figures, doses are shown as gray levels in steps of 200 centiGray (1 Gray = 1 joule/kg).

The quantitative dose values at the vertices of the brain stem B in 5 cross-sections, for both paths, are given in Table 1. The first column contains point labels. The second and fourth columns show the dose values for the manually planned path and the computed path, respectively, in centiGray (cGy). The third and fifth columns show these values in percent of the dose deposited at the center of the sphere approximating the tumor. A non-zero dose is computed in some vertices of B for the automatically planned path, despite the fact that nowhere along this path the beam intersects B. The radiation dose close to the theoretical cylinder modeling the beam is not exactly null. The dosimetry program makes use of a model of the beam that takes this into account. Our planner could use a similar model, but would then regularly fail to find a path when the tumor is too close to a critical region.

An elevated relative dose is obtained for vertices close to the tumor, mainly at points BrStem.5.1, BrStem.4.2, and BrStem.3.1. Table 1 shows that the dose at these points is reduced in the computed path by 46%, 55% and 76%, respectively, relatively to the manually planned path. The table shows a substantial dose reduction ratio at all other vertices, but these reductions are less critical since the doses in cGy for the manually generated paths are significantly lower.

	manually planned motion		computedmotion	
BrStem.1.1	177.8	8.9	80.9	4.1
BrStem.l.2	76.7	3.8	10.8	0.5
BrStem.l.3	13.7	0.7	0.0	0.0
BrStem.l.4	14.5	0.7	0.0	0.0
BrStem.l.5	42.5	2.1	1.4	0.1
BrStem.2.1	161.0	8:0	23.9	1.2
BrStem.2.2	121.7	6.1	25.8	1.3
BrStem.2.3	60.7	3.0	1.6	0.1
BrStem.2.4	33.2	1.7	0.0	0.0
BrStem.2.5	32.6	1.6	0.0	0.0
BrStem.3.1	239.5	12.0	55.0	2.8
BrStem.3.2	60.3	3.0	0.5	0.0
BrStem.3.3	68.5	3.4	1.7	0.1
BrStem.3.4	37.0	1.9	0.0	0.0
BrStem.3.5	144.2	7.2	18.6	0.9
BrStem.3.6	90.9	4.5	6.0	0.3
BrStem.3.7	38.7	1.9	0.0	0.0
BrStem.3.8	38.5	1.9	0.0	0.0
BrStem.4.1	163.2	8.2	19.4	1.0
BrStem.4.2	242.6	12.1	106.6	5.4
BrStem.4.3	43.8	2.2	1.2	0.0
BrStem.4.4	30.6	1.5	0.0	0.0
BrStem.4.5	30.0	1.5	0.0	0.0
BrStem.4.6	40.6	2.0	0.3	0.0
BrStem.5.1	313.4	15.7	165.6	8.4
BrStem.5.2	88.2	4.4	50.2	2.5
BrStem.5.3	8.0	0.4	0.0	0.0
BrStem.5.4	11.1	0.6	0.0	0.0
BrStem.5.5	89.9	4.5	30.1	1.5
	(a)	(b)	(c)	(d)

Table 1: Comparison of energy doses in the brain stem (Case 1)

7.2. CASE 2

Fig. 7 shows the CT image of an axial cross-section of the brain for Case 2. Two critical regions B (brain stem) and OC (optic nerve and chiasm) are delineated by polygons. The tumor is designated by ***T.*** Again both the manually generated path and the automatically computed path consist of 4 connected arcs in different planes. The tumor was approximated by a single sphere.

Fig. 8 and 9 show the energy distribution computed by the dosimetry program in the cross-section shown in Fig. 7. Table 2 compares dose values at the vertices of the critical regions.

8. CONCLUSION

This paper describes a planner developed to help a surgeon generate satisfactory paths for a radiation beam used with radiosurgery. Using geometric techniques, this planner avoids irradiating critical regions of the brain. Experiments demonstrate

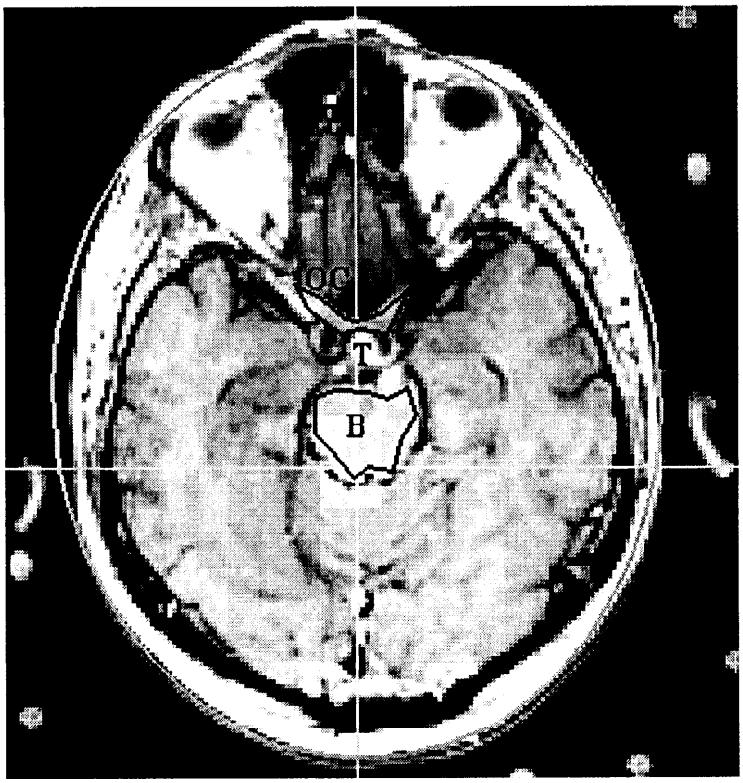

Figure 7: Axial cross-sect ion of the brain in Case 2

that it reduces the path planning time involved in radiosurgery and improves energy deposition.

Beyond the immediate improvements brought by this automatic planner, we envision that significant future progress can be done along the following two directions:

- For some locations of a tumor (relative to critical regions), the constraints of the LINAC system seriously reduce the quality of the radiosurgery treatment. Better treatment could be achieved by using a system allowing arcs in both vertical and non-vertical planes. Such a system would make manual planning harder, but this difficulty can be eliminated by an automatic planner. Automatic planning might motivate the development of new more flexible radiosurgical systems.

- In the longer term, faster and more reliable image interpretation techniques will make it possible to directly connect image acquisition to beam control with limited surgeon intervention. This could make it possible to eliminate the painful stereotaxic frame attached to the patient's head. It could also allow the

Figure 8: Energy deposition for the manually generated path (Case 2)

application of radiosurgery to the destruction of tumors in parts of the human body which are more difficult to localize in space, e.g., liver and pancreas.

Stereotaxic radiosurgery of brain tumors is one instance of so-called "bloodless surgery", for which there is markedly growing interest. We expect that computer-based motion planning techniques such as those described above, together with image interpretation techniques, will facilitate further development of this safer, less painful, and more cost effective type of surgery.

References

[1] Cohen,I., Cohen, L., and Ayache, N. 1992. Using deformable surfaces to segment 3D images and infer differential structures. *Proc. CCA 1992, Lecture Notes in Computer Science* 558, Sandini (ed.), Springer Verlag, New York, NY, 648-652.

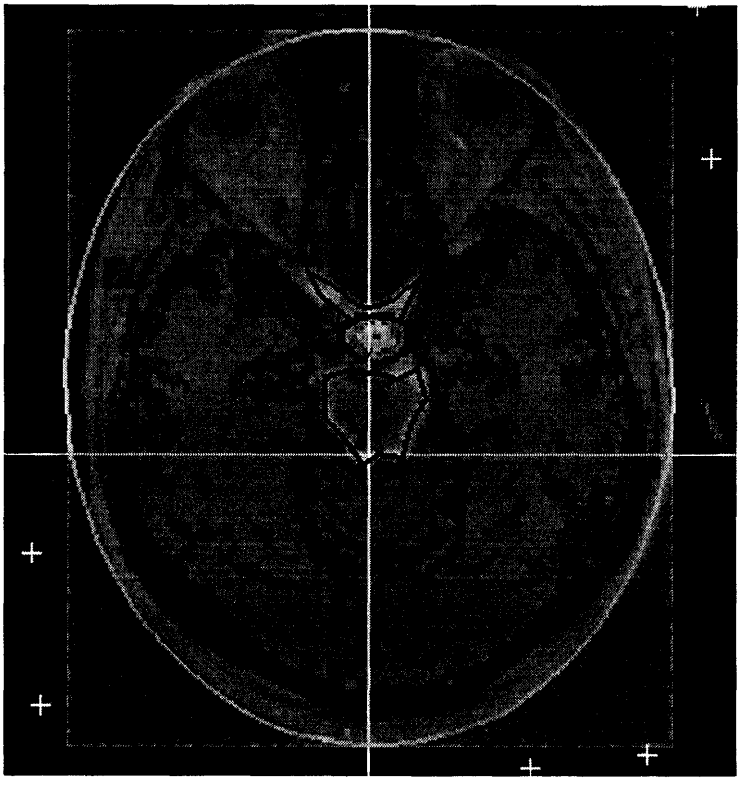

Figure 9: Energy deposition for the automatically planned path (Case 2)

[2] Edelsbrunner, H. and Guibas, L. 1989. Topologically sweeping an arrangement. ***J. of Computer and System Sciences,*** 38:165–194.

[3] Guibas, L. and Seidel, R. 1986. Computing convolution by reciprocal search. *Proc.* ***of the ACM Symp. on Computational Geometry,*** Yorktown Heights, NY, 90-99.

[4] Latombe, J.-C. 1991. ***Robot motion planning.*** Kluwer, Boston, MA, 1991.

[5] Lavallée, S. et al. 1992. Image guided operating robot: a clinical application in stereotactic neurosurgery. *Proc.* ***IEEE*** *Conf.* ***Robotics and Automation,*** Nice, France, 618-624.

[6] Leitner, F. and Cinquin, P. 1991. Dynamic segmentation: detecting complex topology 3D objects. *Proc.* ***IEEE Int. Conf. on Engineering in Medicine, Biology and Society,*** Orlando, FL, 295-296.

[7] Lozano-Perez, T. 1983. Spatial planning: A configuration space approach. ***IEEE Tr. on Computers,*** 32(***2):*** 108-120.

	manually planned motion		computedmotion	
OptNerve.	27.8	1.4	0.0	0.0
OptNerve.	173.3	8.7	24.3	1.2
OptNerve.	159.8	8.0	14.5	0.7
OptNerve.	46.3	2.3	0.0	0.0
OptNerve.	57.4	2.9	0.4	0.0
OptNerve.	35.9	1.8	0.0	0.0
OptNerve.	140.9	7.0	4.1	0.2
OptNerve.	199.0	9.9	29.1	1.5
BrStem.3	146.7	7.3	3.3	0.2
BrStem.3	200.5	10.0	7.9	0.4
BrStem.3	70.0	3.5	0.5	0.0
BrStem.3	24.8	1.2	0.0	0.0
BrStem.3	21.7	1.1	0.0	0.0
BrStem.3	17.8	0.9	0.0	0.0
BrStem.3	19.4	1.0	0.0	0.0
BrStem.3	17.9	0.9	0.0	0.0
BrStem.3	24.0	1.2	0.0	0.0
BrStem.3	31.1	1.6	0.0	0.0
BrStem.3	116.0	5.8	8.1	0.4
BrStem.3	104.0	5.2	0.6	0.0
Chiasm.3	322.1	16.1	229.8	11.5
Chiasm.3	404.3	20.2	219.0	11.0
Chiasm.3	364.9	18.2	248.3	12.4
Chiasm.3	135.3	6.8	6.1	0.3
Chiasm.3	174.0	8.7	23.5	1.2
	(a)	(b)	(c)	(d)

Table 2: Comparison of energy doses in Case 2

[8] Lutz, W., Winston, K. R., and Maleki, N. 1988. A System for stereotactic radiosurgery with a linear accelerator. ***Int. J. Radiation Oncology*** *Biol.* ***Phys.,*** 14:373-381.

[9] Paul, H.A. et al. 1992. A surgical robot for total hip replacement surgery. *Proc.* ***IEEE Conf. Robotics and Automation,*** Nice, France, 606-611.

[10] Welzl, E. 1991. ***Smallest enclosing disks.*** Technical Report B 91-09, Institut für Informatik, FU Berlin.

[11] Winston, K. R. and Lutz, W. 1988. Linear accelerator as a neurosurgical tool for stereotactic radiosurgery. ***Neurosurgery,*** 22(3):454–464.